THE JOURNAL OF PHYSICAL CHEMISTRY A

 VOLUME 110, NUMBER 6, FEBRUARY 16, 2006

ARTICLES

Systematic Behavior of Charge-Transfer Transitions and Energy Level Variation in Soft Donor Complexes of the Trivalent Lanthanides

G. K. Liu,*,† M. P. Jensen,† and P. M. Almond†,‡

Chemistry Division, Argonne National Laboratory, Argonne, Illinois 60439, and Department of Civil Engineering and Geosciences, University of Notre Dame, South Bend, Indiana 46556

Received: October 13, 2005; In Final Form: December 1, 2005

The systematic behavior of the charge-transfer (CT) energies in mixed 2,2′-bipyridyl (bipy), *N*,*N*-diethyldithiocarbamate (Et_2dtc^-) complexes of the trivalent lanthanides, $Ln(Et_2dtc)_3(bipy)$, is investigated to understand the electronic structure of f-element complexes containing soft donor ligands. The energies of ligand to Ln^{3+} CT are extremely low in this system, an effect attributed to the presence of the soft donor ligands. The lowest CT energy level for the Sm^{3+}, Eu^{3+}, and Yb^{3+} complexes falls into the visible range. In $Eu(Et_2dtc)(bipy)$, the Eu^{3+} ion becomes nonluminescent because the CT energy stretches below the metastable $^5D_0$ electronic state, whereas luminescence from the CT state and the $4f^{13}$ $^2F_{5/2}$ state are observed in the Yb compound. The variation in the energy of the lowest level CT transition for the entire $Ln(Et_2dtc)_3(bipy)$ series has been evaluated using the experimentally determined CT levels of the Sm^{3+}, Eu^{3+}, and Yb^{3+} compounds based on the systematic behavior of the lanthanides, which is invariant with respect to the type of ligand. The energy difference between the ground electronic states of the lanthanide ions and the ligand-centered valence band may also be calculated from these results.

I. Introduction

The location of lanthanide energy levels relative to the valence band and conduction band in inorganic materials is often critical to the material's properties for applications. For example, dipole-allowed f−d transition luminescence of Ce^{3+} provides an efficient scintillation in phosphors; however, the f−d transitions of Eu^{2+} are only efficient for scintillation when autoionization of the excited 5d electrons into the conduction band is eliminated.[1] Charge-transfer (CT) measurements are useful tools for characterizing and understanding the electronic properties of lanthanide containing materials because the energy required for ligand-to-metal CT in compounds containing trivalent lanthanides is a measure of the location of the ground state of the divalent lanthanide ions relative to the top of the valence band.[2] As such, CT measurements provide an effective method for determining the locations of the 4f energy levels of lanthanide ions relative to the valence and conduction bands of host complexes.

Lanthanide CT has been studied extensively, particularly in Eu^{3+}-doped compounds. A systematic change in CT energy with type of lanthanide was revealed previously in several systems. Jörgensen first investigated the CT energies for bromide complexes of trivalent Sm, Eu, Tm, and Yb in ethanol.[3] Barnes and Pincott[4] and also Blasse and Bril[5] found that the CT band of Sm^{3+} in solids always appears 1.1 ± 0.1 eV higher than that of Eu^{3+}. More recently, lanthanide CT energies were investigated by Krupa and co-workers[6,7] and van Piterson et al.[8,9] Comparison also has been made between CT energies of Eu^{3+} and that of Yb^{3+} in crystals.[2]

* E-mail: gkliu@anl.gov.
† Argonne National Laboratory.
‡ University of Notre Dame.

10.1021/jp0558674 CCC: $33.50
Published on Web 01/21/2006

Ligand-to-metal CT transitions in lanthanide compounds usually occur in the UV region, higher than 4 eV, or 32 000 cm^{-1}.[2] In some compounds that contain so-called soft donor ligands, such as CaS[10] or $((C_6H_5)_3PH)_3LnI_6$,[11] the CT energy level falls below 4 eV for Sm^{3+}, Eu^{3+}, and Yb^{3+}, the most easily reduced Ln^{3+} ions. Because of this, the energies and dynamics of the ligand-to-metal CT reactions provide an opportunity to examine the electronic structures of lanthanide complexes with ligands containing donor atoms that are softer than oxygen. For example, Ionova et al. have used the CT energies of Eu^{3+} in solution-phase complexes containing both hard oxygen donor and soft sulfur donor ligands to probe the origins of chemical selectivity in complexes being considered for the chemical separation of trivalent lanthanide and actinide ions.[12,13]

We are interested in identifying the specific electronic differences between the 4f, lanthanide (Ln), and 5f, actinide (An), elements in homologous soft donor compounds. Although the Ln^{3+} and An^{3+} have very similar chemistries with hard donor ligands, which prefer ionic bonding over covalent bonding, their chemistries differ for ligands containing donor atoms softer than oxygen (i.e., soft donor ligands).[14] This effect is generally attributed to a modest enhancement of covalence in the An−ligand bonds as compared to the lanthanides, which produces thermodynamically more stable An−soft donor complexes.[15,16] But none of the proposed electronic origins of the suspected enhanced covalence in actinide−soft donor ligand bonds have been experimentally verified. The mixed-ligand coordination compounds of the lanthanides $Ln(Et_2dtc)_3(bipy)$ with the formula $LnC_{25}H_{38}N_5S_6$ ($Et_2dtc^- = N,N$-diethyldithiocarbamate; bipy = 2,2′-bipyridyl), containing two different types of actinide-selective soft donor ligands provide a platform for directly and systematically comparing the electronic and structural properties of trivalent lanthanides and actinides in equivalent complexes. The Sm^{3+}, Eu^{3+}, and Yb^{3+} complexes are expected to have CT energies similar to the iodide- or sulfur-containing materials mentioned above, since the central Ln^{3+} ion is coordinated to eight soft donor atoms, the six sulfurs from three Et_2dtc^- ligands, and two nitrogens from the bipy ligand. We have recently reported the crystal-field energy level structure and excited-state dynamics of $Sm(Et_2dtc)_3(bipy)$, which support the characterization of these ligands as soft donors in this system.[17] To our knowledge, no studies of CT transitions in this system have been reported.

In this paper, we report the systematic behavior of the CT energies in the lanthanide complexes $Ln(Et_2dtc)_3(bipy)$. The CT energies of Ln^{3+} are extremely low in this system. The lowest CT energy level for Sm^{3+}, Eu^{3+}, and Yb^{3+} falls into visible range. This is particularly noteworthy as the Eu^{3+} ($4f^6$) ion in $Eu(Et_2dtc)_3(bipy)$ becomes nonluminescent because the CT energy stretches below the metastable $^5D_0$ state, whereas the CT energy of its actinide homologue, $Am^{3+}(5f^6)$ in $Am(Et_2dtc)_3(bipy)$, is much higher and luminescence from Am^{3+} is observed. We evaluated the variation of the lowest energy CT transition across the entire $Ln(Et_2dtc)_3(bipy)$ series using the experimentally determined CT energies. These results were used to locate the ground-state energy levels of the Ln^{3+} and Ln^{2+} ions relative to the top of the valence (ligand) band of the complex, based on the systematic behavior of lanthanides, which is invariant with respect to the type of compounds or the degree of covalent character in the bonds.[18]

II. Experimental Section

Materials. Single crystals of $Ln(Et_2dtc)_3(bipy)$ (Figure 1, Ln = Sm, Eu, Yb) were synthesized from a 1:3:1 mixture of hydrated lanthanide perchlorate, diethylammonium diethyldithiocarbamate (98%, Aldrich), and 2,2′-bipyridine (99+%, Aldrich) in acetonitrile according to the procedure of Su et al.[19] High-quality, air-stable, single crystals with typical dimensions of 0.1−0.5 mm on a side precipitated from the solutions over the course of hours to days. Because of the intense absorption bands of $Eu(Et_2dtc)_3(bipy)$, crystals of $Gd(Et_2dtc)_3(bipy)$ doped with 1% Eu also were prepared and studied.

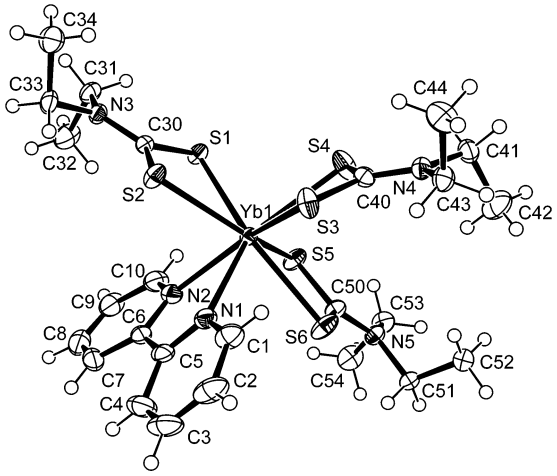

Figure 1. Molecular structure of $Yb(Et_2dtc)_3(bipy)$. Thermal ellipsoids are shown at the 50% probability level.

Single-Crystal X-ray Diffraction. A single crystal of $Yb(Et_2dtc)_3(bipy)$ was mounted on a glass fiber, cooled to −100 °C with a Bruker KRYO-FLEX, and optically aligned on a Bruker APEX II charge-coupled device X-ray diffractometer using a digital camera. Intensity data were measured using graphite monochromated Mo Kα radiation from a sealed tube and monocapillary collimator. APEX II software (v 1.0-22, Bruker AXS) was used for preliminary determination of the cell constants and data collection control. The intensities of reflections of a sphere were collected by a combination of four sets of exposures. Each set had a different ϕ angle for the crystal, and each exposure covered a range of 0.3° in ω. A total of 2400 frames were collected with an exposure time of 30 s.

The determination of integral intensities and global refinement were performed using SAINT+ (v 7.09, Bruker AXS) with a narrow-frame integration algorithm. A semiempirical absorption correction was subsequently applied using SADABS.[20] SHELXTL (v 6.14) was used for space group determination (XPREP), direct methods structure solution (XS), and least-squares refinement (XL).[21] The crystal was assigned to the monoclinic space group, $P2_1/c$, based on Laue class and systematic absences. The structure was solved via direct methods and refined by full-matrix least squares on F^2. The final refinements included anisotropic displacement parameters for all non-hydrogen atoms. Hydrogen atoms were placed at idealized positions and refined using a riding model constraint with displacement parameters set at 1.2 U_{eq} of the attached carbon atom (1.5 U_{eq} for CH_3 groups). The crystallographic details and selected bond lengths and angles for $Yb(Et_2dtc)_3(bipy)$ are given in Tables 1 and 2, respectively. Atomic coordinates and equivalent isotropic displacement parameters are included as Supporting Information.

Spectroscopic Measurements. To obtain the emission and excitation spectra of the Ln^{3+} ions, a pulsed Nd^{3+}−YAG laser at 355 nm was used directly or to pump a tunable dye laser. The samples were mounted in an Oxford cryostat with temperature control from 2 to 295 K. The fluorescence emission was dispersed by a monochromator (SPEX 1704) at a spectral

TABLE 1: Crystallographic Data for $Yb(Et_2dtc)_3(bipy)$

compound	$Yb(Et_2dtc)_3(bipy)$
formula mass	774.01
cryst size (mm)	$0.301 \times 0.064 \times 0.062$
space group	$P2_1/c$ (no. 14)
a (Å)	17.414(1)
b (Å)	10.5109(7)
c (Å)	17.231(1)
β (°)	96.324(1)
V (Å^3)	3134.6(4)
Z	4
T (°C)	−100
λ (Å)	0.71073
max 2θ (°)	67.40
obsd data $I > 2\sigma(I)$	9700
ρ_{calc} (g cm^{-3})	1.640
μ(Mo Kα) (cm^{-1})	34.07
$R(F)$ for $F_0^2 > 2\sigma(F_0^2)^a$	0.0250
$R_w(F_0^2)^b$	0.0526

[a] $R(F) = \sum||F_0| - |F_c||/\sum|F_0|$. [b] $R_w(F_0^2) = [\sum[w(F_0^2 - F_c^2)^2]/\sum wF_0^4]^{1/2}$.

TABLE 2: Selected Bond Lengths (Angstroms) and Angles (Degrees) for $Yb(Et_2dtc)_3(bipy)$

Yb(1)−N(1)	2.528(2)	S(1)−C(30)	1.725(2)
Yb(1)−N(2)	2.497(2)	S(2)−C(30)	1.715(2)
Yb(1)−S(1)	2.7663(5)	S(3)−C(40)	1.726(2)
Yb(1)−S(2)	2.7712(5)	S(4)−C(40)	1.706(2)
Yb(1)−S(3)	2.8366(5)	S(5)−C(50)	1.715(2)
Yb(1)−S(4)	2.7699(5)	S(6)−C(50)	1.718(2)
Yb(1)−S(5)	2.8408(5)	N(3)−C(30)	1.334(2)
Yb(1)−S(6)	2.7254(5)	N(4)−C(40)	1.333(2)
C(5)−C(6)	1.472(3)	N(5)−C(50)	1.336(2)
N(1) −Yb(1)−N(2)	64.97(6)	S(1)−C(30)−S(2)	117.4(1)
S(1)−Yb(1)−S(2)	64.13(1)	S(3)−C(40)−S(4)	117.2(1)
S(3)−Yb(1)−S(4)	62.99(2)	S(5)−C(50)−S(6)	118.0(1)
S(5)−Yb(1)−S(6)	63.79(2)	Yb(1)−N(1)−C(5)	119.6(1)
N(1)−Yb(1)−S(3)	82.30(4)	Yb(1)−N(2)−C(6)	120.8(1)
N(2)−Yb(1)−S(4)	150.68(4)	N(1)−C(5)−C(6)	117.2(2)
S(1)−Yb(1)−S(5)	79.40(1)	N(2)−C(6)−C(5)	116.2(2)
S(2)−Yb(1)−S(6)	151.37(2)		

resolution of approximately 0.008 nm and detected with a cooled RCA C31034 photomultiplier. The signals were recorded using a gated boxcar (Stanford Research Systems, model SR250). The fluorescence decay measurements were performed using a digital storage oscilloscope (Tektronix TDS 680C). The emission spectra have been calibrated based on the various grating and PMT efficiencies at different wavelengths. To measure the absorption spectra, single crystals (about 10−15 wt %) were ground and pressed into a pellet with KBr powder. The pellet was mounted in the cryostat and UV−vis−IR absorption spectra of samples were collected with a computer-controlled Cary-14 spectrophotometer (OLIS, Inc.).

III. Theoretical Basis of CT

CT from the ligand-centered valence band to a trivalent lanthanide occurs when a photon is absorbed, causing both an electronic transition and lattice relaxation. Before a CT transition, the initial electronic state of the complex has the Ln^{3+} ion in its ground state $4f^n$ configuration and the ligand populating any of the valence band states. After absorption of a photon, the system transits into an excited CT state where the central lanthanide ion is in a divalent, $4f^{n+1}$, configuration and a hole (L^+) is left in the surrounding ligands. The configuration coordinate diagrams shown in Figure 2 illustrate the electronic transitions and lattice relaxation involved in CT absorption and luminescence emission for three lanthanide ions (Sm^{3+}, Eu^{3+}, and Yb^{3+}) in $Ln(Et_2dtc)_3(bipy)$ crystals. Each of the configuration coordinate diagrams in Figure 2 is based on the experimental results to be discussed below.

An important characteristic of CT transitions in Ln^{3+} compounds is that the systematic variation in CT energies between different lanthanides is independent of the type of complexes. This means that, if the CT energy is determined by calculations or actual measurements for at least one Ln^{3+} ion, one can predict the CT energies for all Ln^{3+} ions with configurations from $4f^1$ to $4f^{13}$ with reasonable accuracy.[2] This property holds true in the present work for the $Ln(Et_2dtc)_3(bipy)$ series with Ln = Sm, Eu, and Yb.

Because the Ln^{3+} CT energy is approximately equal to the energy gap between the ground-state level of Ln^{2+} and the top of the valence band of the complex, the fixed difference between the energy of CT to a trivalent lanthanide ion and that of another ion can be exploited to locate the ground state of both the divalent and trivalent lanthanide ions. Since Eu^{3+} has the lowest CT energy of the Ln^{3+} ions, occurring in the near UV or even in the visible range in the case of $Eu(Et_2dtc)_3(bipy)$, one may use the measured CT energy for Eu^{3+} to determine the CT energy for all other Ln^{3+} ions, which is the energy of the Ln^{2+} ground state relative to the top of the valence band. Therefore, the ground-state energy level of a $Ln^{2+}(4f^{n+1})$ ion relative to the valence band of a complex L, $E_{Vf}(n+1, 2+, L)$, can be obtained from

$$E_{Vf}(n+1,2+,L) = E_{Vf}(7,2+,L) + \Delta E_{Vf}(n+1,7,2+) \quad (1)$$

where $E_{Vf}(7,2+,L)$ is the energy difference between the Eu^{2+} ground state and the valence band of complex L, and $\Delta E_{Vf}(n+1,7,2+)$ is the ligand-independent energy difference between Eu^{2+} and a divalent lanthanide ion with a $4f^{n+1}$ configuration.

Because E_{Vf} of a divalent $4f^{n+1}$ ion is approximately equal to the CT energy of the trivalent ion in $4f^n$ configuration, eq 1 may also be expressed as

$$E_{Vf}(n+1,2+,L) \approx E^{CT}(n,3+,L) = E^{CT}(6,3+,L) + \Delta E^{CT}(n,6,3+) \quad (2)$$

where $E^{CT}(n,3+,L)$ is the lowest CT energy of a trivalent lanthanide ion (in a $4f^n$ configuration) in complex L and $\Delta E^{CT}(n,6,3+)$ is the difference in the CT energy between Eu^{3+} and another trivalent lanthanide ion in a $4f^n$ configuration.

IV. Results and Discussion

A. Crystal and Molecular Structure of $Yb(Et_2dtc)_3(bipy)$. The importance of the lanthanide−ligand distance in determining the electronic properties of these lanthanide complexes was demonstrated in our prior analysis of the crystal field levels of $Sm(Et_2dtc)_3(bipy)$.[17] To ensure that the coordination environments of the $Ln(Et_2dtc)_3(bipy)$ complexes are uniform across the lanthanide series and that any differences in the lanthanide−ligand distances are caused solely by the differences in cation radii, we determined the crystal structure of $Yb(Et_2dtc)_3(bipy)$ by X-ray diffraction. The crystal structures of the corresponding Sm and Eu compounds at room temperature have already been reported,[22,23] as have the structures of $Pr(Et_2dtc)_3(bipy)$[24] and $Er(Et_2dtc)_3(bipy)$.[19]

Bright-yellow $Yb(Et_2dtc)_3(bipy)$ (Figure 1) is isostructural with the four $Ln(Et_2dtc)_3(bipy)$ compounds with known crystal structures. The crystal is composed of discrete $Yb(Et_2dtc)_3(bipy)$ molecules containing octacoordinate Yb atoms. As observed in the analogous lanthanide compounds, each metal ion is coor-

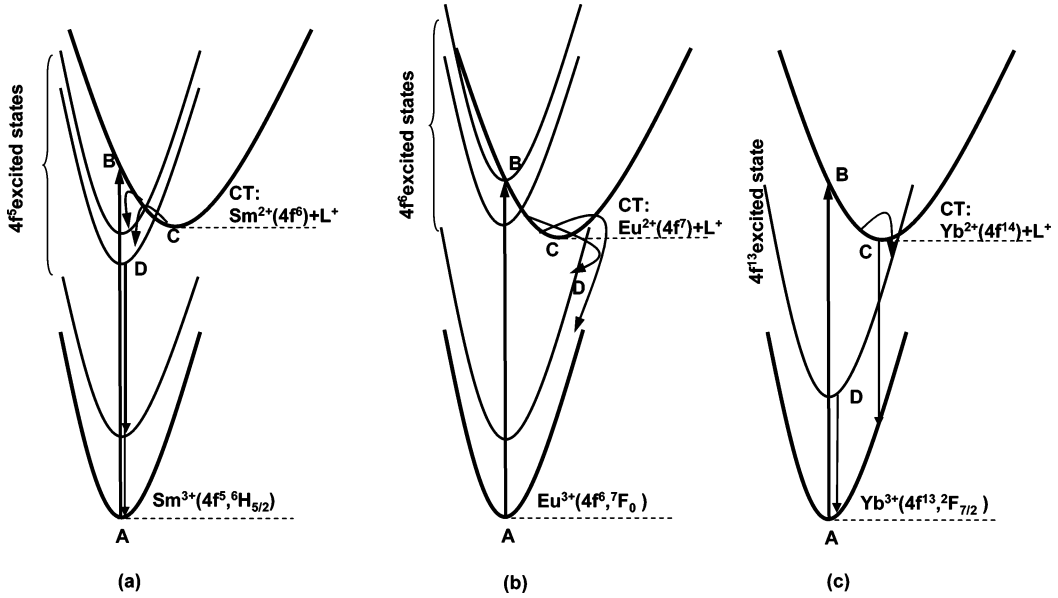

Figure 2. Configuration coordinate diagram illustrating the electronic transition and lattice relaxation involved in CT absorption in trivalent lanthanide ions in $Ln(Et_2dtc)_3(bipy)$ crystals. The thicker parabolic curves corresponds to the ground-state energies of Ln^{3+} and Ln^{2+}, respectively, while the thinner curves represent the excited states of Ln^{3+} ions.

dinated to six sulfur atoms from three bidentate Et_2dtc^- ligands and two nitrogen atoms from a bidentate bipyridyl ligand. The Yb−S distances range between 2.725 and 2.841 Å with an average distance of 2.785 Å. The average Yb−N distance is 2.513 Å. The average Yb−S and Yb−N distances are shorter than those of the analogous compounds of the lighter lanthanides but are exactly those expected from the lanthanide contraction, suggesting little difference in the covalent contribution to the Ln-ligand bonds across the lanthanide series.[25−27] The S−Yb−S and N−Yb−N angles within each coordinated ligand also are, necessarily, slightly larger than those observed in the compounds of the lighter lanthanides. The bond lengths and bond angles within each ligand are consistent from lanthanide to lanthanide, and are unremarkable.

The packing of the $Ln(Et_2dtc)_3(bipy)$ molecules within the crystal consistently places the lanthanides in a low-symmetry, distorted dodecahedral coordination environment. Each of the bidentate Et_2dtc^- ligands adopts a conformation with one shorter and one longer Ln−S distance. This places the lanthanides, including Yb, in a site of formally C_1 symmetry with respect to the ligands' S and N donor atoms. The low symmetry is reinforced by a small twist in the Et_2dtc^- ligand trans to the bipy. Ignoring this minor distortion, the local symmetry at the metal center can be approximated as C_s, though we have had success in modeling the spectrum of $Sm(Et_2dtc)_3(bipy)$ with even higher approximations of the local site symmetry.[17]

B. Absorption Spectra of CT and 4f−4f Transitions. The absorption spectrum of Sm^{3+} in the $Sm(Et_2dtc)_3(bipy)$-KBr pellet was recorded at room temperature and liquid helium temperature. Figure 3 shows the UV−vis absorption from the $4f^5\ {}^6H_{5/2}$ ground state. A broad and intense peak appears with its low-energy shoulder at 26 000 cm^{-1}, which is due to the ligand−Sm^{3+} CT absorption. The weaker and much narrower peaks are identified and attributed to transitions to the $4f^5$ excited states of Sm^{3+}. These f−f absorption transitions are nominally spin forbidden but are actually weakly allowed as intermediate-coupling admixtures into both the $^6H_{5/2}$ and the terminal quartet's wave functions via spin−orbit interactions. A detailed analysis of the crystal-field energy levels of the $4f^5$ states has been reported.[17] It was shown that the spectroscopic properties of

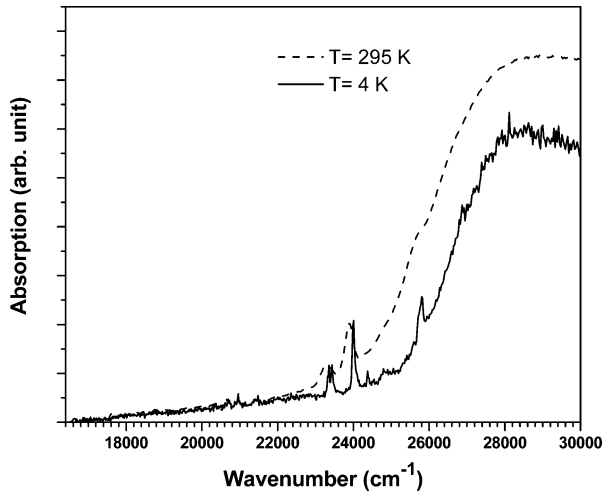

Figure 3. Absorption spectra of $Sm(Et_2dtc)_3(bipy)$ at 295 and 4 K.

the 4f−4f lines that overlap with the CT band above 23 000 cm^{-1} are significantly different from the 4f−4f lines in the lower-energy region. Apparently, as shown in Figure 3, the 4f lines with energies higher than 23 000 cm^{-1}, which overlap the CT bands, are much stronger than those in the lower-energy region. The relative intensities of the high-energy 4f−4f transitions are quite inconsistent with those calculated using the Judd−Ofelt theory. Moreover, the positions of the 4f−4f lines in the higher-energy region do not match the predicted values obtained from crystal-field modeling based on a single charge ion−ligand interaction model.[17] We believe that the discrepancies in both the intensity and energy level position of the high-energy 4f−4f lines result from coupling to CT states. A strong coupling between the 4f electrons and ligand electrons are excluded in both crystal-field theory and Judd−Ofelt theory.

The influence of CT states on the spectrum and excited-state dynamics of Eu^{3+} in $Eu(Et_2dtc)_3(bipy)$ is even stronger than that of the Sm^{3+} system. Absorption spectra of $Eu(Et_2dtc)_3(bipy)$ at 295 and 77 K are shown in Figure 4. The low-energy shoulder of the CT band stretches below 17 000 cm^{-1}. Thus the 4f−4f transitions from the $Eu^{3+}\ {}^7F_0$ ground state to the $^5D_{0,1,2,3}$ and

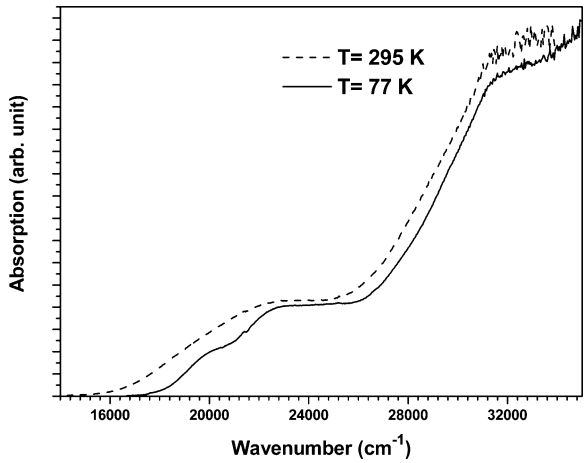

Figure 4. Absorption spectra of $Eu(Et_2dtc)_3(bipy)$ at 295 and 77 K.

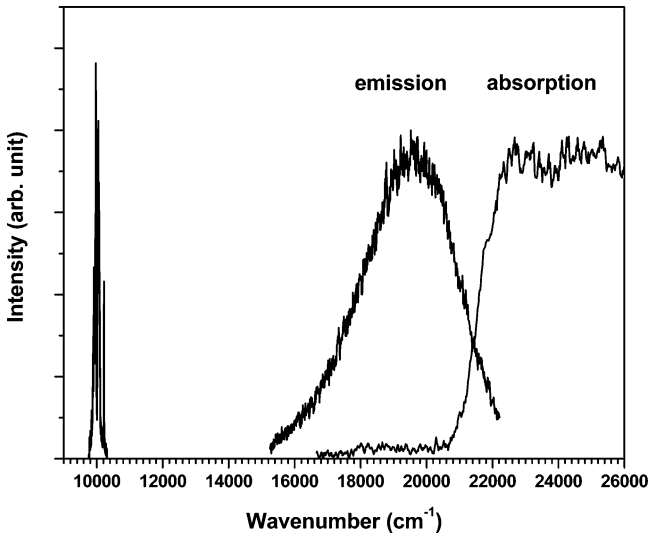

Figure 5. CT absorption and emission spectra of $Yb(Et_2dtc)_3(bipy)$ at 4 K. The group of sharp peaks centered at 10 000 cm^{-1} is the emission spectrum of the 4f−4f transition from the $^2F_{5/2}$ excited state to the $^2F_{7/2}$ ground state of Yb^{3+}.

$^5L_6$ states are expected to overlap with the CT band in the region from 17 000 to 25 000 cm^{-1}. Three very weak, sharp lines on top of the CT band are visible at 17 656, 21 410, and 25 180 cm^{-1} in spectra recorded at 77 K or lower temperatures (Figure 4). These lines are presumably 4f−4f transitions suppressed by interference from the CT transitions. Because first-order crystal-field splitting is absent in the $^8S_{7/2}$ ground state of the Eu^{2+} $4f^7$ configuration and the first excited state is far above the ground state, the splitting of the $^8S_{7/2}$ state should be small.[28,29] Therefore, the lowest-energy Eu^{3+} CT transition should be comparatively narrow, and CT to the Eu^{2+} excited states is not expected to occur below 40 000 cm^{-1}. Consequently, the absorption band observed below 28 000 cm^{-1} in $Eu(Et_2dtc)_3(bipy)$ arises from the CT transition, while the much stronger absorption band above 28 000 cm^{-1}, which is also observed in $Gd(Et_2dtc)_3(bipy)$, is attributed to the complexed ligands.

In $Yb(Et_2dtc)_3(bipy)$, the CT transition initiates both CT luminescence and luminescence from the $4f^{13}$ excited state. The Yb system, therefore, provides more detailed information on the energy level structure and excited-state dynamics. As shown in Figure 5, the low-energy shoulder of the Yb^{3+} CT band at 4 K is located at approximately 21 500 cm^{-1}. At room temperature it shifts to 19 500 cm^{-1}. The broad emission band centered at 19 700 cm^{-1} is due to radiative relaxation of the excited CT state, while the sharp lines centered at 10 000 cm^{-1} are fluorescence transitions from the $^2F_{5/2}$ state of Yb^{3+}. The three spectra in Figure 5 are not on the same scale. In fact, the 4f−4f emission lines are at least 2 orders of magnitude stronger than the direct CT luminescence, which indicates that population of the excited $4f^{13}$ states is more efficient than the radiative relaxation back to the Yb^{3+} ground state.

In general, both the 4f states of lanthanides and the 5f states of actinides in compounds are localized electronic states and their coupling to ligand states is primarily ionic. Nevertheless, there are chemical differences in the complexes of Ln^{3+} and An^{3+} cations with ligands containing soft donor atoms, which are generally attributed to a modestly larger covalent component in the An−ligand bonds as compared to the lanthanides.[14−16] To compare ion−ligand coupling in lanthanide compounds to that in actinide compounds, we also synthesized $Am(Et_2dtc)_3(bipy)$ and probed the electronic energy levels of Am^{3+}, which has a $5f^6$ configuration electronic structure similar to the $4f^6$ of Eu^{3+}. It is surprising that fluorescence from Am^{3+} was observed with laser excitation at room temperature, and that the CT transition occurs at 22 750 cm^{-1}, which is far above the metastable $^5D_1$ emitting state of the $5f^6$ ion and much higher than the CT energy of Eu^{3+}. These results indicate that An^{3+} ions are likely more redox stable than Ln^{3+} in this complex, because of the larger energy gap between the ligand-centered valence band and the ground-state energy levels of the divalent actinides as compared to that of the lanthanides. This is fully consistent with the greater difficulty in reducing lighter (pre-californium) trivalent actinide ions, such as Am^{3+},[30,31] to the divalent state and the generally higher energy of the 5f orbitals of the An^{3+} ions relative to the 4f orbitals of the homologous Ln^{3+}.[32]

C. Dynamics of CT Transitions: Lattice Relaxation and Electron−Hole Binding. The ligand-to-lanthanide CT transitions appear as intense absorption bands because they are spin- and dipole-allowed transitions, which are much stronger than the parity-forbidden, lanthanide-centered 4f−4f transitions. Once the CT transition terminates at the ground state of the divalent lanthanide ion, a series of strong, dynamic relaxation processes brings the system to the minimum in its configuration coordinate. Because the ionic radius of a divalent lanthanide is approximately 0.18 Å larger than the radius of the original trivalent lanthanide,[27] both complex electronic and lattice relaxation processes may occur. In the three complexes we studied, based on the experimental results, relaxation may occur by several routes illustrated in Figure 2.

(1) Intersystem crossing back to the initial parabola of configuration coordinate with quenching of all luminescence. This is the case we observed for the Eu complex. No fluorescence was observed in laser excitation of $Eu(Et_2dtc)_3(bipy)$, whereas most compounds containing Eu^{3+}, including other dithiocarbamate complexes such as $Na[Eu(Me_2dtc)_4]$,[33] and numerous 2,2′-bipyridine-based complexes[34−37] are luminescent. The origin of this anomaly is well understood in the present case because the emitting state, $^5D_0$, is above the low-energy shoulder of the CT band. Radiative transitions from the $^5D_0$ state are quenched and nonradiative relaxation through the ^7F_J states as well as direct interconfiguration relaxation from the CT state is expected.

(2) Intersystem crossing to the excited states of the trivalent ion, followed by intraconfigurational 4f−4f transitions to the ground state. This is the situation we observed in $Sm(Et_2dtc)_3(bipy)$, as typified by the strong fluorescence from the $^4G_{5/2}$ excited state at 17 687 cm^{-1}. The observed fluorescence decay

of the $^4G_{5/2}$ manifold is single exponential, with a lifetime of 24.5 μs, indicating the presence of a single Sm^{3+} site in the lattice. By use of Judd−Ofelt theory, values of three intensity parameters were obtained ($\Omega_{2,4,6} = 1.57$, 2.65, and 3.65, in units of 10^{-20} cm^{-1}). The calculated branching ratios for transitions from the $^4G_{5/2}$ manifold are in agreement with experimental values. The calculated radiative lifetime of the $^4G_{5/2}$ manifold is 3.24 ms, and the corresponding fluorescence quantum efficiency is only 0.75%, which may be due to efficient multiphonon relaxation processes induced by the localized high-frequency vibrational modes in the bipyridyl group. The thermal line broadening and shifts of the $^4G_{5/2}(1) \rightarrow {}^6F_{1/2}$ transition also were observed and fitted very well by the McCumber−Sturge equations with an assumption of Raman phonon-scattering processes as the leading relaxation mechanism.[17]

(3) Radiative relaxation back to the ground-state parabola of the configuration coordinate and to the excited 4f states of the trivalent ion. This is the case we observed for the Yb complex, as shown by the spectra in Figure 5. In fact, for lanthanide compounds, radiative CT relaxation back to the initial parabola of the configuration coordinate occurs only in Yb complexes. In most cases, CT emission to both the $^2F_{7/2}$ and $^2F_{5/2}$ states of Yb^{3+} occurs. However, for $Yb(Et_2dtc)_3(bipy)$, we observed only the emission to the $^2F_{7/2}$ state. CT emission to the upper $4f^{13}$ multiplet, $^2F_{5/2}$, was not observed. This indicates that the gap between the lowest CT state of $Yb(Et_2dtc)_3(bipy)$ and the $^2F_{5/2}$ energy level is small enough that the transition falls into the IR region.

The multiband structure in the low-temperature absorption spectrum of $Eu(Et_2dtc)_3(bipy)$ is clearly apparent in Figure 4. The total CT bandwidth is approximately 5000 cm^{-1}, which is consistent with typical values of lanthanide CT bands, which range between 5000 and 10 000 cm^{-1}.[2,8,9] Because of overlap with ligand absorption bands and the limitation of our spectrometer in UV region, we cannot determine the bandwidth of the CT band for $Sm(Et_2dtc)_3(bipy)$ or $Yb(Et_2dtc)_3(bipy)$. However, the bandwidth of the CT emission spectrum of $Yb(Et_2dtc)_3(bipy)$ shown in Figure 5, is only about 3000 cm^{-1}, which is much narrower than the CT absorption bandwidth. Therefore the difference between the emission bandwidth and the absorption bandwidth indicates that the excited CT state is more complicated than the single-well parabolic configuration coordinate depicted in Figure 2.

The multiband structure of the low-temperature CT spectrum of Eu^{3+} also suggests that the CT transitions may end up in different electronic states separated by approximately 2000−3000 cm^{-1}. Because the excited states of Eu^{2+} are more than 20 000 cm^{-1} above the ground state and the ground-state splitting is expected to be much smaller than 2000 cm^{-1},[28,29] the multiple Eu^{3+} CT bands likely arise from differences in the electronic structures of the sulfur-bearing Et_2dtc^- ligands and the nitrogen-bearing bipyridyl ligand. This also implies the presence of multiwell parabolic configuration coordinates for $Eu(Et_2dtc)_3(bipy)$. Such multiwell excited-state energy potentials are not unusual when CT vibronic excitons are taken into account.[38−40] Moreover, the excited-state potentials shown in Figure 2 may not be simple single-well parabolas because of dynamic lattice distortions induced by the CT transitions.

D. Systematics of Energy Level Variations. The measured values of the low-energy shoulder of the CT transitions for Eu^{3+}, Sm^{3+}, and Yb^{3+} in $Ln(Et_2dtc)_3(bipy)$ at liquid helium temperature are listed in Table 3. For comparison, these values are plotted in Figure 6 with the reported CT energies of the same cations in four other compounds.[2] By use of the CT energy of

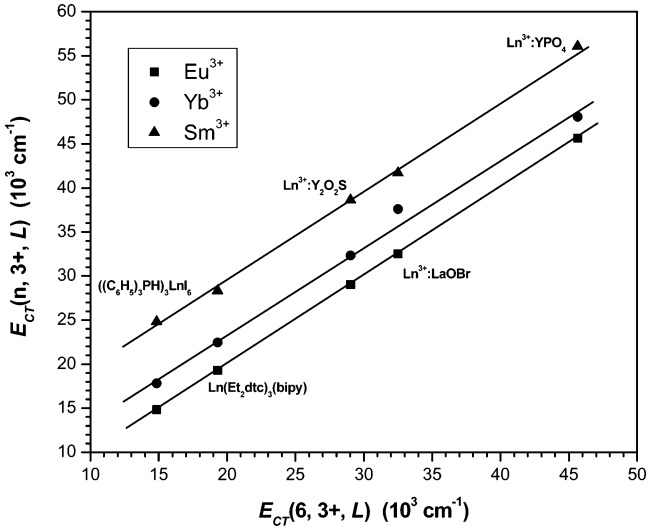

Figure 6. Comparison of energy levels of the lowest CT state of Sm^{3+}, Eu^{3+}, and Yb^{3+} in various compounds.

TABLE 3. Measured CT Energies for $Ln(Et_2dtc)_3(bipy)$ at 4 K

Ln^{3+} in $Ln(Et_2dtc)_3(bipy)$	$E^{CT}(Ln^{3+})$ (10^3 cm^{-1})
Sm^{3+}	22.5
Eu^{3+}	19.3
Yb^{3+}	28.3

Eu^{3+} compounds as a reference, the CT energies of Sm^{3+} and Yb^{3+} in these sets of compounds locate nicely on two lines parallel to that of the Eu^{3+} line. Although the CT energies of a given Ln^{3+} differ by as much as 30 000 cm^{-1} from $((C_6H_5)_3PH)_3LnI_6$ to Ln^{3+}:YPO_4, the energy differences between different lanthanides are independent of the compounds, the concentration of the absorbing species, the type of ligand (i.e., hard vs soft ligands), and even whether the crystal contains discrete molecules or extended coordination networks. Whereas the difference in CT energy between different lanthanides in the same compound is a characteristic of the 4f elements being compared, the variation of the CT energy in different compounds of the same Ln^{3+} ion shown in Figure 6 is caused by differences in the ion−ligand coupling strength and the chemical stability of the systems.

According to eq 2, the systematic variation of the Ln^{3+} CT energies, or the ground-state energy levels of Ln^{2+} relative to the valence band of $Ln(Et_2dtc)_3(bipy)$, can be calculated using the values of $\Delta E_{Vf}(n+1,7,2+)$ given by Dorenbos[2] and our measured value of the Eu^{3+} CT energy. The results are plotted in Figure 7. The agreement between the calculated energies and the experimentally measured CT energies of $Sm(Et_2dtc)_3(bipy)$ and $Yb(Et_2dtc)_3(bipy)$ underscores the general applicability of the results across the lanthanide series even in the case of the presumably more covalent Ln−S- and Ln−N-containing compounds, where ion−ligand electronic coupling could be important.

By comparison of the CT absorption and emission spectra of $Yb(Et_2dtc)_3(bipy)$ (Figure 5), one can see that both the emission bandwidth and the red shift from the absorption bands are on the order of 3000 cm^{-1} (<0.4 eV). This broadening and energy shift are expected considering the change in the configuration coordinate between the divalent and trivalent ions in the complex. On the other hand, as indicated in Figure 2c, the CT relaxation to the $^2F_{5/2}$ excited state of Yb^{3+} and the ensuing narrow fluorescence band arising from intraconfigurational 4f−4f transitions also suggest that the energy difference

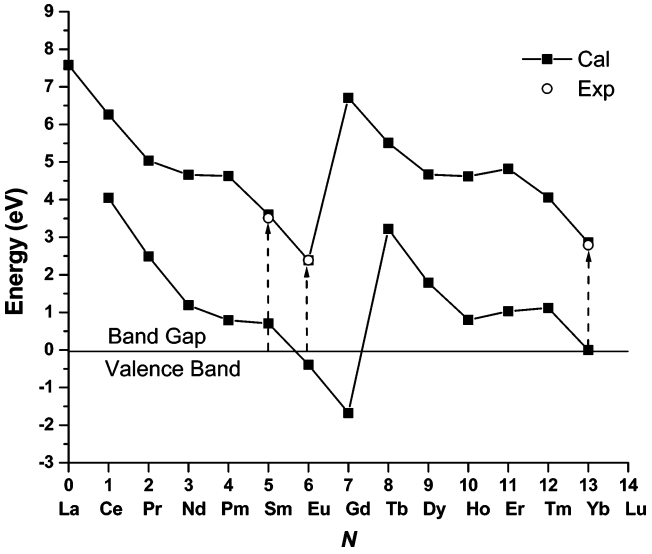

Figure 7. Systematic variation of the ground-state energies of Ln^{2+} (upper points) and Ln^{3+} (lower points) relative to the valence band of $Ln(Et_2dtc)_3(bipy)$. Values calculated based on the measured CT energies of Eu^{3+} and Yb^{3+} in $Ln(Et_2dtc)_3(bipy)$.

between the Yb^{3+} ground state and the top of the valence band should be less than 0.2 eV, one-half of the observed CT bandwidth. This observation, coupled with the complex independent variation of the energy levels of Ln^{3+} relative to the valence band,[2] allows us to determine the locations of the ground states of each Ln^{3+} relative to the valence band of the complex. The predicted systematic variation is shown in Figure 7.

The chemical picture that emerges from our measurements provides a basis for comparing the degree of f-state ligand interaction in the ground state by combining the spectroscopic and structural information. On the basis of the calculations summarized by Figure 7, the ground $4f^n$ states of Eu, Gd, and Yb lie at or below the highest-occupied ligand states. The ground-state energies of the other lanthanides range from ca. 0.6 to as much as 4 eV above the top of the ligand band. Despite the varying energy mismatch between the metal 4f and the filled ligand orbitals for some of the lanthanides (most notably Ce, Pr, Tb, and Dy), the structures and chemistry of the compounds are constant across the series, suggesting that any covalent interactions involving filled ligand orbitals and empty f orbitals are weak. Since the ground state energies of most of the lanthanides lie above the highest-occupied ligand states, it might seem more likely to observe covalence incorporating significant 4f orbital participation between occupied metal orbitals and empty ligand orbitals, for example, metal−ligand back-bonding. Yet this does not seem to be the case either. The crystal structures of the $Ln(Et_2dtc)_3(bipy)$ complexes provide no evidence of such back bonding in our complexes. Moreover, although such behavior has been reported for complexes of the light actinides with π-acceptor soft donor ligands, it has not been observed in similar lanthanide complexes,[41−43] and interactions with the lanthanide-centered 5d orbitals appear to dominate bonding in triscyclopentadienyl complexes of Ln^{3+}.[32] Thus the combined structural and CT spectroscopic evidence imply that any covalent bonding involving f orbitals in the $Ln(Et_2dtc)_3(bipy)$ complexes is weak.

Nevertheless, as suggested by the variation in CT energies summarized in Figure 6, the energy difference between the ground or excited metal ion states and the ligand valence states is a sensitive function of the chemical environment, even among these comparatively ionic species. The CT energies we measured for the $Ln(Et_2dtc)_3(bipy)$ complexes are quite different from those reported for Ln^{3+} ions doped in YPO_4,[2] even though the energy gaps between the ligand-based valence states and the $4f^n$ ground state of the Ln^{3+} ions are very similar for the two systems. In contrast, the $4f^n$ ground states of Ln^{3+} doped in CaF_2 all lie above the valence states,[2] while for Ln^{3+}-doped YAG, only the $4f^n$ states of Ce^{3+}, Pr^{3+}, and Tb^{3+} lie above the top of the valence band.[18,44] Since each of these cases places the Ln^{3+} ions in octacoordinate O or F sites, the measured relative positions of the ground $4f^n$ and ligand electronic states are not solely dependent on the nature of the ligand donor atoms (i.e., hard, ionic O and F donors vs softer N and S donors). Such ligand effects should not be important when comparing a homologous series of isostructural f-element compounds, such as $Ln(Et_2dtc)_3(bipy)$ and $An(Et_2dtc)_3(bipy)$, however.

V. Conclusions

The systematic variation of the CT transition energies in lanthanide compounds provides a useful tool for understanding the electronic structure of the complexes by locating the relative position of the ground-state energy levels of the Ln^{2+} and the Ln^{3+} ions with respect to the highest-occupied ligand orbitals. Even in a system containing soft donor ligands, the differences in CT energies between different Ln^{3+} are independent of the compound. Therefore, the CT energies of all Ln^{3+} ions in the same compound can be predicted based on the measured value for one ion. The measured values of the ligand-to-metal CT energies for Ln^{3+} in $Ln(Et_2dtc)_3(bipy)$ are extremely low in comparison with other systems, an expected behavior that reflects the properties of the soft donor complex. The systematic behavior also implies that the degree of covalent interaction between the ligands and the Sm^{3+}, Eu^{3+}, and Yb^{3+} ions are similar despite their widely differing ion size (ca. 0.09 Å)[27] and the differences in the ground-state energy of the 4f states.

By measurement of the energies of the CT transitions, the present work provides a clear explanation for the total quenching of Eu^{3+} 4f−4f fluorescence in $Eu(Et_2dtc)_3(bipy)$, whereas luminescence from other lanthanide ions, Sm^{3+} and Yb^{3+}, and an actinide ion, Am^{3+}, in the same complex could be observed. The comparison between the excited-state dynamics of Eu^{3+} in the $4f^6$ configuration and Am^{3+} in the $5f^6$ configuration highlights distinct differences in the cation−ligand electronic coupling of the lanthanides and actinides in this series of complexes. Our observations and analysis provide a detailed understanding of electronic interactions and the effects of covalency of f-element ions coordinated with soft donor ligand complexes, giving a benchmark for further studies of the electronic structures of the complexes of trivalent lanthanides and actinides with soft donor ligands.

Acknowledgment. Work at Argonne National Laboratory, operated by the University of Chicago, was performed under the auspices of the U.S. Department of Energy, Office of Basic Energy Sciences, Division of Chemical Sciences, Geosciences and Biosciences, under Contract No. W-31-109-ENG-38.

Supporting Information Available: Table of atomic coordinates and displacement parameters for $Yb(Et_2dtc)_3(bipy)$ and an X-ray crystallographic file for $Yb(Et_2dtc)_3(bipy)$ in CIF format. This material is available free of charge via the Internet at http://pubs.acs.org.

References and Notes

(1) Blasse, G.; Schipper, W.; Hamelink, J. J. *Inorg. Chim. Acta* **1991**, *189*, 77.

(2) Dorenbos, P. *J. Phys.: Condens. Matter* **2003**, *15*, 8417.

(3) Jörgensen, C. K. *Molecular Physics* **1962**, *5*, 271.
(4) Barnes, J. C.; Pincott, H. *J. Chem. Soc. A* **1966**, 842.
(5) Blasse, G.; Bril, A. *Phys. Lett.* **1966**, *23*, 440.
(6) Krupa, J. C. *J. Alloys Compd.* **1995**, *225*, 1.
(7) Gerard, I.; Krupa, J. C.; Simoni, E.; Martin, P. *J. Alloys Compd.* **1994**, *207/208*, 120.
(8) van Pieterson, L.; Reid, M. F.; Wegh, R. T.; Meijerink, A. *J. Lumin.* **2001**, *94/95*, 79.
(9) van Pieterson, L.; Reid, M. F.; Burdick, G. W.; Meijerink, A. *Phys. Rev. B* **2002**, *65*, 045114.
(10) Yamashita, N.; Asano, S. *J. Phys. Soc. Jpn.* **1987**, *56*, 352.
(11) Ryan, J. L. *Inorg. Chem.* **1969**, *8*, 2053.
(12) Ionova, G.; Ionov, S.; Rabbe, C.; Hill, C.; Madic, C.; Guillaumont, R.; Krupa, J. C. *Solvent Extr. Ion Exch.* **2001**, *19*, 391.
(13) Ionova, G.; Ionov, S.; Rabbe, C.; Hill, C.; Madic, C.; Guillamont, R.; Modolo, G.; Krupa, J. C. *New J. Chem.* **2001**, *25*, 491.
(14) Nash, K. L. *Solvent Extr. Ion Exch.* **1993**, *11*, 729.
(15) Diamond, R. M.; Street, K.; Seaborg, G. T. *J. Am. Chem. Soc.* **1954**, *76*, 1461.
(16) Jensen, M. P.; Bond, A. H. *J. Am. Chem. Soc.* **2002**, *124*, 9870.
(17) Chen, X. Y.; Jensen, M. P.; Liu, G. K. *J. Phys. Chem. B* **2005**, *109*, 13991.
(18) Thiel, C. W.; Cruguel, H.; Sun, Y.; Lapeyre, G. J.; Macfarlane, R. M.; Equall, R. W.; Cone, R. L. *J. Lumin.* **2001**, *94*, 1.
(19) Su, C.; Tang, N.; Tan, M.; Yu, K. *Polyhedron* **1996**, *15*, 233.
(20) Sheldrick, G. M. *SADABS*; Univeristy of Göttingen: Germany, 2004.
(21) Sheldrick, G. M. *SHELXTL*; Bruker AXS, Inc.: Madison, WI, 1997.
(22) Varand, V. L.; Glinskaya, L. A.; Klevtsova, R. F.; Larionov, S. V. *J. Struct. Chem.* **1998**, *39*, 244.
(23) Varand, V. L.; Glinskaya, L. A.; Klevtsova, R. F.; Larionov, S. V. *J. Struct. Chem.* **2000**, *41*, 544.
(24) Bower, J. F.; Cotton, S. A.; Fawcett, J.; Highes, R. S.; Russell, D. R. *Polyhedron* **2003**, *22*, 347.
(25) Brown, I. D.; Shannon, R. D. *Acta Crystallogr.* **1973**, *A29*, 266.
(26) Shannon, R. D.; Vincent, H. *Struct. Bonding* **1974**, *19*, 1.
(27) Shannon, R. D. *Acta Crystallogr.* **1976**, *A32*, 751.
(28) Liu, G. K.; Beitz, J. V.; Huang, J. *J. Chem. Phys.* **1993**, *99*, 3304.
(29) Levin, L. I.; Eriksonas. *J. Phys. C.: Solid State Phys.* **1987**, *20*, 2081.
(30) Morss, L. R. The Lanthanides. In *Standard Potentials in Aqueous Solution*; Bard, A. J., Parsons, R., Jordan, J., Eds.; Marcel Dekker: New York, 1985; pp 587−629.
(31) Martinot, L.; Fuger, J. The Actinides. In *Standard Potentials in Aqueous Solution*; Bard, A. J., Parsons, R., Jordan, J., Eds.; Marcel Dekker: New York, 1985; pp 631−673.
(32) Strittmatter, R. J.; Bursten, B. E. *J. Am. Chem. Soc.* **1991**, *113*, 552.
(33) Kobayashi, T.; Naruke, H.; Yamase, T. *Chem. Lett.* **1997**, 907.
(34) Sinha, S. P. *Spectrochim. Acta* **1964**, *20*, 879.
(35) Filipescu, N.; Bjorklund, S.; McAvoy, N.; Degnan, J. *J. Chem. Phys.* **1968**, *48*, 2895.
(36) Ulrich, G.; Ziessel, R.; Manet, I.; Guardigli, M.; Sabbatini, N.; Fraternali, F.; Wipff, G. *Chem.−Eur. J.* **1997**, *3*, 1815.
(37) Tsaryuk, V.; Zolin, V.; Legendziewicz, J.; Szostak, R.; Gawryszewska, P. *J. Alloys Compd.* **2004**, *380*, 418.
(38) Agranovich, V. M.; Zakhidov, A. A. *Chem. Phys. Lett.* **1977**, *50*, 278.
(39) Vikhnin, V. S. *Solid State Commun.* **2003**, *127*, 283.
(40) Vikhnin, V. S.; Eglitis, R. I.; Kapphan, S. E.; Borstel, G.; Kotomin, E. A. *Phys. Rev. B* **2002**, *65*, 104304.
(41) Mazzanti, M.; Wietzke, R.; Pécaut, J.; Latour, J. M.; Maldivi, P.; Remy, M. *Inorg. Chem.* **2002**, *41*, 2389.
(42) Berthet, J. C.; Rivière, C.; Miquel, Y.; Nierlich, M.; Madic, C.; Ephritikhine, M. *Eur. J. Inorg. Chem.* **2002**, 1439.
(43) Mehdoui, T.; Berthet, J. C.; Thuéry, P.; Ephritikhine, M. *J. Chem. Soc., Dalton Trans.* **2005**, 1263.
(44) Thiel, C. W.; Cruguel, H.; Wu, H.; Sun, Y.; Lapeyre, G. J.; Cone, R. L.; Equall, R. W.; Macfarlane, R. M. *Phys. Rev. B* **2001**, *64*, 085107.